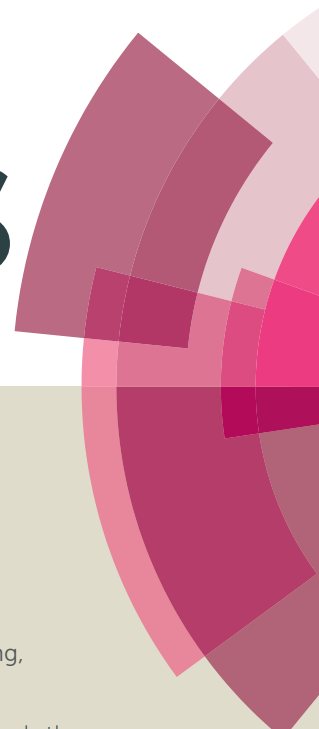


RSC Advances



This article can be cited before page numbers have been issued, to do this please use: S. Chen, L. Wang, X. Dong, X. Liu, J. Zhou, J. Yang and L. Zha, *RSC Adv.*, 2016, DOI: 10.1039/C6RA04247C.



This is an *Accepted Manuscript*, which has been through the Royal Society of Chemistry peer review process and has been accepted for publication.

Accepted Manuscripts are published online shortly after acceptance, before technical editing, formatting and proof reading. Using this free service, authors can make their results available to the community, in citable form, before we publish the edited article. This *Accepted Manuscript* will be replaced by the edited, formatted and paginated article as soon as this is available.

You can find more information about *Accepted Manuscripts* in the [Information for Authors](#).

Please note that technical editing may introduce minor changes to the text and/or graphics, which may alter content. The journal's standard [Terms & Conditions](#) and the [Ethical guidelines](#) still apply. In no event shall the Royal Society of Chemistry be held responsible for any errors or omissions in this *Accepted Manuscript* or any consequences arising from the use of any information it contains.



PAPER

Fabrication of monodisperse Au@Ag bimetallic nanorods loaded nanofibrous membrane with fast thermo-responsiveness and its use as a smart free-standing SERS substrate†

Received 00th January 20xx,
Accepted 00th January 20xx

DOI: 10.1039/x0xx00000x

www.rsc.org/

Siyuan Chen,^a Liying Wang,^a Xu Dong,^b Xiaoyun Liu,^{c*} Jianfeng Zhou,^c Jianmao Yang^c and Liusheng Zha^{a,c*}

A novel type of metal nanoparticles loaded smart nanofibrous membrane with fast thermo-responsiveness was fabricated by electrospinning the aqueous solution containing poly(N-isopropylacrylamide-co-N-hydroxymethylacrylamide) and monodisperse Au@Ag bimetallic nanorods with core-shell structure, followed by heat treatment. The results obtained by electron microscopy show that the anisotropic nanoparticles are oriented along the axes of its constituent nanofibers. The produced membrane has high stability in aqueous medium and remarkable thermo-responsiveness. It takes less than 10 seconds to reach its deswelling or swelling equilibrium state with the temperature jumping or plunging between 25 °C and 50 °C. The smart nanofibrous membrane with macroscopic mechanical strength is able to be used as a free-standing surface enhanced Raman scattering (SERS) substrate with high Raman signal reproducibility for quantitative analysis, and its SERS efficiency can be readily elevated by raising detection temperature across its phase transition temperature due to its fast thermo-response rate. Particularly, since the composite nanofibrous membrane possesses catalysis for the reduction of 4-nitrothiophenol to 4-aminothiophenol by NaBH₄, it has the ability to in-situ SERS monitor the reaction, and it was deduced from the detected intermediate that the reaction proceeds via a condensation reaction route.

Introduction

In recent years, metal nanoparticles loaded stimulus responsive composite materials have attracted more and more attention due to their prominent characteristics, i.e., the properties of the loaded nanoparticles can be tuned by external stimulus or the stimulus can be sensed by detecting their properties change.¹⁻⁴ Therefore, the smart composite materials have fascinating potential applications in many fields, such as sensor, actuator, biomedicine, catalysis, etc.^{1,4-6} Up to date, the smart polymer materials used for loading metal nanoparticles have been

stimulus responsive bulky hydrogels and microgels (including nanogels) with nanometer to micrometer size.^{4,5,7} It is known that smart bulky hydrogels have much slower stimulus-response than smart microgels due to the estimation that the response rate is inversely correlated to their size.⁸ Since fast stimulus-response of smart materials is important to their applications, such as tunable catalysis, sensing or detection, actuation, drug delivery,^{1,9} smart microgels are preferentially used for loading metal nanoparticles.^{4,5,10,11} For example, in our group, pH and/or temperature responsive microgels have been utilized for loading Ag or Au nanoparticles, and the produced composite microgels were used as smart catalysts or surface enhanced Raman scattering (SERS) substrates with temperature-controllable activity.¹²⁻¹⁵ However, smart microgels usually exist as colloidal particles in aqueous solution, so they suffer from poor colloidal stability and no macroscopic morphology and mechanical strength for use in some device like sensor or actuator. Moreover, when used as catalysts, they are difficult to be recycled by facile process. Hence, developing new type of smart polymer material for loading metal nanoparticles, which has both macroscopic mechanical strength and fast stimulus-response, is of important practical significance.

Stimulus responsive nanofibrous membrane is the smart polymer material which consists of orderly or randomly aligned nanofibers of tens to hundreds of nanometers diameters.¹⁶

^a State Key Laboratory for Modification of Chemical Fibers and Polymer Materials & College of Materials Science and Engineering, Donghua University, Shanghai 201620, P. R. China. E-mail: lszha@dhu.edu.cn

^b State Key Laboratory of Molecular Engineering of Polymers and Department of Macromolecule Science, Fudan University, Shanghai 200433, P. R. China.

^c Research Center for Analysis and Measurement, Donghua University, Shanghai 201620, P. R. China. E-mail: xyliu@dhu.edu.cn

†Electronic Supplementary Information (ESI) available: See DOI: 10.1039/x0xx00000x

Compared to smart bulky hydrogel, it has much faster stimulus-response owing to their constituent ultra thin fibers and porous structure helpful for the transfer of the stimulus to the whole material. Its reported applications have demonstrated that the smart material allows for convenient use in a device because of their macroscopic mechanical strength and flexible morphology.^{17,18} If used as the carrier for nanocatalysts, it can be readily recovered from the reaction system.^{19,20} The nanofibrous membrane is usually produced by electrospinning technique, which features simplicity, flexible morphology tuning and wide variety in usable polymers.^{19,21,22} Therefore, it could be expected that stimulus responsive electrospun nanofibrous membrane is the substitute of smart bulky hydrogel and microgel for loading metal nanoparticles.

Within the field of metal nanoparticles-based nanoscience and nanotechnology, the bimetallic nanoparticles with core-shell structure have evolved increasing interest due to their superior physicochemical, optical and catalytic properties as compared to their respective monometallic analogues.^{23,24} Among them, the bimetallic nanorod based on gold nanorod (AuNR) core and silver shell (Au@AgNR) is particularly attractive because of its potential applications in surface enhanced Raman scattering (SERS) substrate, catalyst, etc.^{23,25,26} Recently, in our group, monodisperse Au@AgNR prepared through seed-mediated growth process by reduction of AgNO₃ using AuNR with narrow size and shape distribution as seed was used as SERS substrate with high Raman signal reproducibility for quantitative analysis.²⁶ Its SERS efficiency is remarkably increased with its Ag shell thickness thanks to the enhancing surface electric field and the chemical enhancement associated with electronic ligand effect. Furthermore, it has been reported that, compared to monometallic Ag nanoparticles, the bimetallic Au@Ag nanoparticles with core-shell structure has much higher chemical stability owing to free electron transfer from the Au core to Ag shell.²⁷ This can avoid weakening Au@AgNRs' SERS efficiency during usage and storage, otherwise their oxidized Ag surfaces hinder the charge transfer to the analyte molecule according to chemical enhancement mechanism.²⁸ In addition to SERS substrates, the nanorods can be used as the nanocatalysts with high catalytic reactivity and selectivity for some chemical reactions owing to the synergistic catalytic effect of their constituent gold and silver components.^{29,30} For example, the results obtained by Monga et al. demonstrated that Au@AgNRs exhibit the selective formation of 3-nitroaniline for the reduction of 1,3-dinitrobenzene as compared to 1,3-phenylenediamine in case of Au and Ag nanorods.³¹

Herein, we report the fabrication of monodisperse Au@AgNRs loaded thermo-responsive composite nanofibrous membrane by electrospinning the aqueous solution containing poly(N-isopropylacrylamide-co-N-hydroxymethylacrylamide) and the nanorods, followed by heat treatment. The observations by electron microscopy confirm that Au@AgNRs are oriented along the axes of its constituent nanofibers. The produced composite nanofibrous membrane with fast thermo-response and stable macroscopic morphology in aqueous medium is able to be used as a smart free-standing SERS substrate with temperature-tunable efficiency. Specially, it was found that it

has the ability to in-situ SERS monitor its catalyzed reaction, which is beneficial to understanding the reaction mechanism.

Experimental

Materials

Hexadecyltrimethylammonium bromide (CTAB, 99%), chloroauric acid trihydrate (HAuCl₄·3H₂O, 99.5%), sodium borohydride (NaBH₄, 95%), silver nitrate (AgNO₃, 99.8%), glycine (99.5%), hydrochloric acid (HCl, 37%), N-hydroxymethylacrylamide (NMA, 98%), 4-nitrothiophenol (4-NTP, 99%), 2,2'-azobis(isobutyronitrile) (AIBN, 99%) and sodium hydroxide (NaOH, analytical grade) were all purchased from Shanghai Chemical Reagent Co. and used as received. L(+)-Ascorbic acid (AA, 99%) was supplied by Acros Organics. Sodium oleate (NaOL, 97%), N-isopropylacrylamide (NIPAM, 95%) were purchased from TCI America. NIPAM was purified by recrystallization from a mixture of toluene and hexane (60:40, V/V). Deionized water used in the synthesis and characterization was made using a Millipore Direct-Q system.

Synthesis of monodisperse Au@AgNRs

Monodisperse AuNRs were synthesized by binary surfactant method reported by Ye et al.³² Then, the AuNRs were used as seeds for the synthesis of monodisperse Au@AgNRs.²⁶ Briefly, to 5 mL of 0.4 M glycine buffer solution at pH = 8.9 (adjusted with 1.0 M NaOH solution), 10 mL of the AuNRs solution and certain volume of 0.01 mM AgNO₃ aqueous solution were added. Subsequently, 400 μL of 0.1 M ascorbic acid aqueous solution was added under gentle magnetic stirring. After 12 h, the solution was centrifuged for 15 min at 6000 rpm, and the supernatant was removed and the precipitate was redispersed in deionized water.

Fabrication of Au@AgNRs loading thermo-responsive composite nanofibrous membrane

Firstly, poly(N-isopropylacrylamide-co-N-hydroxymethylacrylamide) (PNN) was synthesized by free radical polymerization in ethanol, as reported by Chen et al.³³ The molar ratio of N-isopropylacrylamide to N-hydroxymethylacrylamide in the feed recipe is 5:1. Then, certain amount of purified Au@AgNRs dispersed in 1 mL of deionized water were added into 3 mL of PNN aqueous solution of 30 wt% concentration, followed by vigorous stirring at room temperature for 24 h to produce the electrospinning solution of Au@AgNRs concentration of 25 nM, 50 nM or 100 nM. Subsequently, the electrospinning solution was loaded into a 10 mL plastic syringe and electrospun at positive voltage of 13 kV, 15 cm working distance (distance between the needle tip and the grounded metal plate), and 0.9 mL/h flow rate for 4 h at room temperature. Finally, the formed nanofibrous membrane was heated at 110 °C for 5 h. Keeping constant the polymer concentration in the spinning solution, three kinds of Au@AgNRs/PNN composite nanofibrous membranes were fabricated by changing the concentration of Au@AgNRs (from 25 nM, 50 nM to 100 nM), which are labeled as HNF-1, HNF-2 and HNF-3, respectively.

Characterization

^1H NMR spectrum of PNN copolymer was measured by a Bruker AV 400 nuclear magnetic resonance spectrometer based on the residual proton resonance of deuterated dimethylsulfoxide (DMSO-d_6). Its number-average molecular weight was obtained by a Brookhaven BI-MWA gel permeation chromatography equipped with light scattering detector using HPLC-grade tetrahydrofuran as eluent.

TEM images of Au@AgNRs/PNN composite nanofibrous membranes were taken with a JOEL 2100F transmission electron microscope at a voltage of 200 kV. The samples were collected on copper grids during electrospinning, followed by heating at $110\text{ }^\circ\text{C}$ for 5 h. Their SEM images were obtained with a Hitachi S-4800 field emission scanning electron microscopy at a voltage of 5 kV. The samples were sputtered with gold.

UV-vis adsorption spectra of diluted Au@AgNRs/PNN composite nanofiber aqueous dispersion at various temperatures were measured from a Perkin Elmer Lambda 35 UV-vis spectrometer with a temperature controller. A quartz cell with 1 cm optical path length was used. Fourier transformation infrared (FTIR) spectra of uncrosslinked PNN nanofibrous membrane and Au@AgNRs/PNN composite nanofibrous membrane were measured with a Thermo Fisher Nicolet 6700 FTIR spectrometer using an ATR attachment with a horizontal Ge crystal.

SERS measurements were performed using a Renishaw inVia-Reflex micro-Raman system equipped with a multi-channel charge-coupled device detector and a DM2500M Leica confocal microscope upon excitation by 532, 633 or 785 nm laser source. All the SERS spectra were the results of 10 s accumulations. In order to assess the SERS efficiency of Au@AgNRs/PNN composite nanofibrous membrane, it (its size: $0.7\text{ cm}\times 0.7\text{ cm}$) was put in the quartz sample cell, then $200\text{ }\mu\text{L}$ of 4-NTP aqueous solution of different concentrations was injected into the cell, followed by recording SERS spectra using Raman microscope with 50X objective. Temperature dependent SERS spectra were measured on a piece of membrane (HNF-3, $0.7\text{ cm}\times 0.7\text{ cm}$) that was immersed in 10^{-9} M 4-NTP aqueous solution in a Linkam THMS600 temperature-controllable cell, which was equilibrated thermally for at least 5 min before SERS measurement.

In situ SERS monitoring catalytic reaction

To test the ability of Au@AgNRs/PNN composite nanofibrous membrane to monitor the catalytic reaction by SERS, the membrane (HNF-2) was immersed in $100\text{ }\mu\text{L}$ of 10^{-4} M 4-NTP aqueous solution, and then $100\text{ }\mu\text{L}$ of 0.1 M NaBH_4 aqueous solution was injected into the sample cell, as schematically illustrated in Fig. 1(b). The reaction progress was monitored by the continuous collection of SERS signals (each scan from 300 cm^{-1} to 1800 cm^{-1} took ca. 5 min) from the membrane surface during the reaction. The reaction temperature in the cell can be controlled as above.

Results and discussion

Fabrication and characterization of Au@AgNRs/PNN composite nanofibrous membranes

The fabrication route of Au@AgNRs loading thermo-responsive composite nanofibrous membrane (Au@AgNRs/PNN composite nanofibrous membrane) is schematically illustrated in Fig. 1(a). Firstly, the fiber forming thermo-responsive polymer, i.e. poly((N-isopropylacrylamide)-co-(N-hydroxymethylacrylamide)) (PNN), was firstly synthesized via azobisisobutyronitrile initiated free radical polymerization in ethanol solution.³³

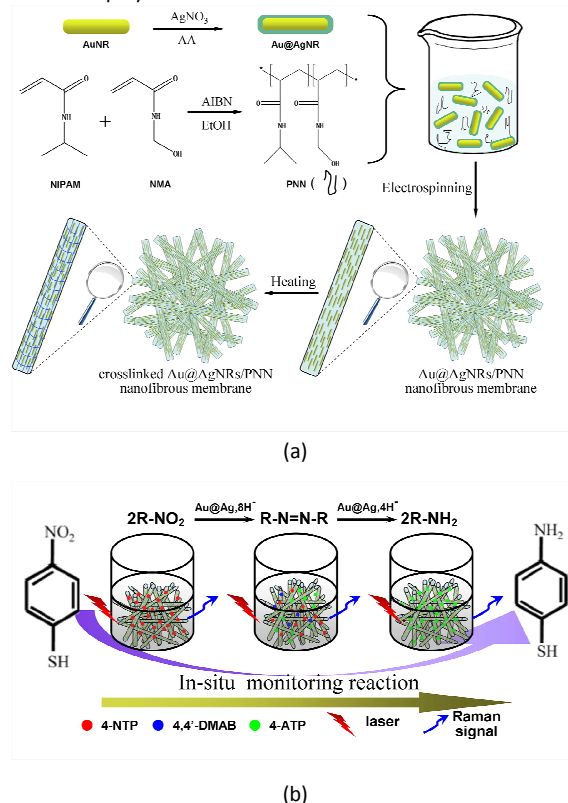


Fig. 1 The fabrication route of thermo-responsive Au@AgNRs/PNN composite nanofibrous membrane (a) and its use in in-situ SERS monitoring catalytic reaction (b)

Its NIPAM/NMA composition determined from its ^1H NMR spectrum (see Fig. S1(a) in the Electronic supplementary information (ESI)[†]) is 100:20.4 (molar ratio), very close to the feeding ratio of 100:20, and its number-average molecular weight estimated by gel permeation chromatography using tetrahydrofuran as eluent is $1.27\times 10^5\text{ g/mol}$. Fig. S1(b) in the ESI[†] shows temperature dependent absorbance (at 500 nm) of the diluted PNN aqueous solution, which exhibits a thermo-responsive hydrophilic-to-hydrophobic phase transition in aqueous medium. Its lower critical solution temperature (LCST) is $41.8\text{ }^\circ\text{C}$, which is remarkably higher than that of poly(N-isopropylacrylamide) ($32\text{ }^\circ\text{C}$), due to the hydrophilicity of its constituting NMA moiety.³⁴ Concurrently, monodisperse Au@AgNRs were prepared and purified by our recently reported method.²⁶ The TEM image of the Au@AgNRs is shown in Fig. S2 (a) in the ESI[†], and we can note that they have excellent monodispersity and well-defined core-shell structure. Their average length and diameter obtained by randomly measuring

50 particles are 81 ± 4 nm and 25 ± 2 nm, with the calculated aspect ratio being 3.2, and the average silver shell thicknesses of their lateral facets and two tips are all 2.7 ± 0.2 nm. The ultraviolet visible (UV-vis) spectrum of the diluted Au@AgNRs aqueous dispersion and its optical image are shown in Fig. S2(b) in the ESI†. According to the previous report,²⁶ the two bands at 708 nm and 505 nm are attributed to the longitudinal and transverse dipolar plasmon mode of Au@AgNRs, respectively, and the band at 385 nm is ascribed to their octupolar plasmon mode. It can also be found from Fig. S2(b) in the ESI† that the longitudinal plasmon band of Au@AgNRs are relatively narrow, further proving their monodispersity. In electrospinning stage, PNN was mixed with Au@AgNRs aqueous dispersion to generate spinning solution after stirring for 24 h. Subsequently, the solution was electrospun at positive voltage of 13 kV, 15 cm working distance (distance between the needle tip and the grounded metal plate), and 0.9 mL/h flow rate at room temperature for 4 h. Finally, the produced nanofibrous membrane was heated at 110°C for 5 h to form crosslinking structure between the polymer chains within its constituent fibers, as illustrated in Scheme S1 in the Supporting Information. The optical images of Au@AgNRs/PNN composite nanofibrous membranes and PNN nanofibrous membrane as control sample are shown in Fig. S3 in the ESI†, and it can be seen that the fabricated products are nonwoven membranes with the area of over 240 cm^2 and the thickness of ca. $60\ \mu\text{m}$, and their colors at dry state change from white to light green with their Au@AgNRs content increasing. Fig. 2 exhibits their scanning electron microscopy (SEM) and transmission electron microscopy (TEM) images of low and high magnification. From their SEM images we can note that these membranes have three-dimensional network structure consisting of lots of randomly deposited fibers, and the fibers are homogeneous in their diameters, without beaded morphology. Their average diameters determined by randomly measuring 50 fibers within each membrane are 806 ± 112 nm, 682 ± 104 nm, 635 ± 34 nm and 607 ± 84 nm, respectively, decreasing with their Au@AgNRs content increasing. This behavior is presumably related to the increase in solution conductivity concomitant to Au@AgNRs incorporation.³⁵ If observing the amplified SEM images of the nanofibers, the bright spots on their surfaces are the Au@AgNRs orienting along their axes, whose amounts are increased with Au@AgNRs concentration in their spinning solution. From their TEM images we can clearly see that the Au@AgNRs are embedded within the fibers and directionally aligned along their axis direction. With the increase in Au@AgNRs content within the nanofibers, the average end-to-end distance between the adjacent nanorods decrease from 146 nm to 89 nm to 41 nm. The low-magnification TEM images show that the oriented alignments are extremely uniform over long distances throughout the whole sample. In contrast to the spinning solution where the Au@AgNRs are randomly dispersed, we can conclude that their oriented alignments inside the nanofibers result from the electrospinning process.³⁶ There are two external fields that trigger such an alignment of the nanorods during the electrospinning process. One is the electric field supplied by the needle, and the other is the flow field formed during the formation of the fibers. When a high voltage was applied to the

spinning solution, the whole solution was polarized. Further, if the repulsive force within the charged solution was larger than its surface tension, a jet would erupt from the tip of the spinneret, producing the flow field. Shortly, the jet entered a bending instability stage, and the nanofibers were formed by the stretch and acceleration of the fluid filament in the instability region as the solvent evaporated. During the formation of nanofibers, the sink-flow effect and strong shear forces were exerted on the Au@AgNRs, leading to their oriented alignment along the flow direction, which is the axial direction of the fibers. Even when a high concentration of the Au@AgNRs (100 nM) was present in the spinning solution, the nanorods were all directionally aligned, which demonstrates that electrospinning is a powerful technique to form oriented alignment of anisotropic nanorods on a large scale.

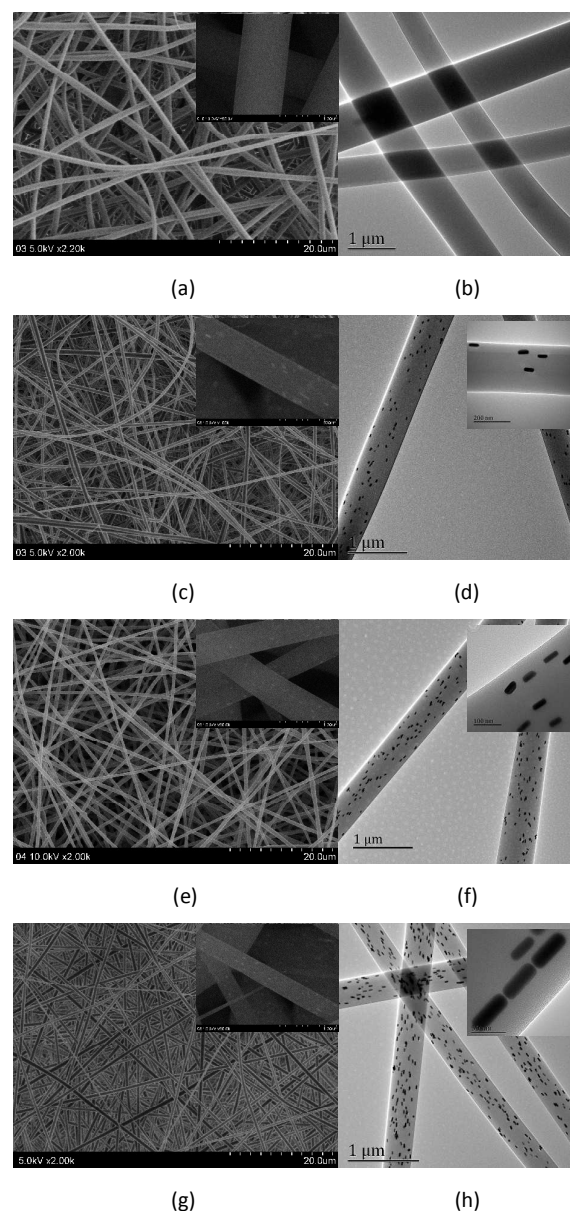


Fig. 2 SEM (left column) and TEM (right column) images of Au@AgNRs/PNN

composite nanofibrous membranes with different Au@AgNRs contents (insets are their magnified images, respectively.) (from top to bottom: control sample ((a) and (b)), HNF-1((c) and (d)), HNF-2 ((e) and (f)) and HNF-3 (g) and (h))

Stability of Au@AgNRs/PNN composite nanofibrous membranes

Obviously, the stability of Au@AgNRs/PNN composite nanofibrous membranes in aqueous medium is important to their application, so it is necessary to evaluate it. For this purpose, about 40 mg of the membrane were immersed in 20 mL water and the solution was oscillated at 100 rpm for 2 h. Fig. S4 in the ESI† shows the optical images of control sample and Au@AgNRs/PNN composite nanofibrous membranes in water before and after oscillation. It can be seen that, after the harsh oscillation, control sample was slightly damaged, whereas the composite membranes were left intact, indicating that they have high stability in water. Hence, it could be speculated that the interactions between Au@AgNRs and PNN polymer are present within the composite nanofibers, which acts as physical crosslinking points. The speculation could be confirmed by the FTIR results, as illustrated in Fig. S5 in the ESI†, which shows the FTIR spectra of uncrosslinked PNN nanofibrous membrane and HNF-2. It can be found by comparing the two spectra that the intensity of 3650 cm^{-1} peak assigned to the O–H stretching mode of NMA units within PNN is significantly decreased for HNF-2, indicating the occurrence of the crosslinking reaction between the polymer chains after heat treatment, as shown in Scheme S1 in the Supporting Information. Moreover, it is worthwhile noting that a small blue shift of amide I and II bands (1650 cm^{-1} and 1530 cm^{-1}) attributed to the amide groups of PNN appears in the spectrum of HNF-2, which may stem from the interactions between the nitrogen atoms in the groups and the Ag atoms on the loaded Au@AgNRs.¹²

Fast thermo-responsive property of Au@AgNRs/PNN composite nanofibrous membranes

Typical optical images of Au@AgNRs/PNN composite nanofibrous membrane immersed in 25 or 50 °C water are exhibited in Fig. 3(a), and it can be seen that its area at 50 °C is much smaller than the one at 25 °C, implying that it possesses remarkable thermo-responsive property. To identify their phase transition temperature, temperature dependent areas of Au@AgNRs/PNN composite nanofibrous membrane in water were measured at a heating rate of $0.1\text{ °C}\cdot\text{min}^{-1}$, and the results are depicted in Fig. 3(b). We can note that all the composite nanofibrous membranes notably shrink with temperature increasing from 25 °C to 50 °C, and their final area shrinking percentages are lowered from 82% to 52% with their Au@AgNRs content rising. They all steeply shrink around 41 °C, i.e. their phase transition temperature, slightly lower than the LCST of PNN. Moreover, the temperature range for the membrane area variation is wider than that for the hydrophilic-to-hydrophobic phase transition of PNN, presumably attributed to inhomogeneous distribution of the crosslinking points inside its nanofibers.³⁷ Further investigation on their thermo-responsive property is to assess their thermo-response rates by measuring the time-dependent areas of the membrane membranes

immersed alternately into the water of 25 or 50 °C after the interval of 2 min, and the results are shown in Fig. 3(c). It is well-known that deswelling of poly(N-isopropylacrylamide) bulky membrane requires a few days to reach the equilibrium state, which is ascribed to the formation of a dense skin layer on the gel surface hindering diffusion of the water.³⁸ In comparison, Au@AgNRs/PNN composite nanofibrous membranes shrunk to deswelling equilibrium state within 2 seconds after a jump in temperature from 25 to 50 °C (see the attached video). On the other hand, they reversibly swelled up to 95% of their initial areas within 10 seconds and reached swelling equilibrium state after the temperature plumped down from 50 to 25 °C. The reversible deswelling-swelling cycle was repeated at least 3 times. With respect to fast stimulus-response rate of smart nanofibrous membrane, it is generally thought to be associated with very small diameters of the constituting nanofibers and porous structure of the membrane, which facilitates the transfer of the stimulus to the whole material.^{9,16} To clarify the reason of their fast and remarkable response to temperature change, we tried to visualize the microstructures of Au@AgNRs/PNN composite nanofibrous membranes at swelling or deswelling equilibrium state comparatively. For this purpose, the equilibrium-swollen nanofibrous membrane in 25 °C or 50 °C water was rapidly transferred into liquid nitrogen for freezing and then freeze dried for SEM observation. The rapid freezing by liquid nitrogen should immobilize the microstructure of the membrane in water and the sizes of its constituent nanofibers. From the SEM images of two freeze dried samples, as shown in Fig. 3(a), we can find that the nanofibers are highly separated with very large mesh structure within the membrane obtained from its equilibrium-swelling state in 25 °C water, whereas they adhere with each other to form bundles of fibers, leading to dense mesh structure within the one from its equilibrium-deswelling state in 50 °C water. If carefully visualizing their amplified SEM images, it can be noted that the nanofibers within the shrunken membrane are slightly thinner than the ones inside the swollen membrane. Thus, we can suppose that the shrinkage of the composite nanofibrous membrane in 50 °C water should mostly arise from adhesion between the nanofibers and formation of fibrous bundles, leading to steep decrease of the free space inside its interior. With regard to what make the nanofibers adhere with each other, we think that it is the hydrophobic interaction between the nanofibers after their polymers undergo temperature-induced hydrophilic-to-hydrophobic phase transition. If too many Au@AgNRs are located on their surfaces, the hydrophobic interactions will be weakened. This is why the area shrinking percentage of Au@AgNRs/PNN composite nanofibrous membranes is lowered with their Au@AgNRs content rising, as depicted in Fig. 3(b).

Subsequently, it is essential to investigate the effect of temperature change on the plasmonic property of the Au@AgNRs embedded within the composite nanofibrous membrane. To this end, a nanofibers aqueous dispersion was prepared by adding small amount of the broken membrane (HNF-2) to water, followed by sonicating the solution for 5 h, and its UV-vis spectra in the range of 300–1100 nm at different temperatures were obtained, as shown in Fig. 3(d). Firstly, the

longitudinal plasmon band of the Au@AgNRs embedded within the membrane becomes broader compared to the one before electrospinning (Fig. S1(b) in the ESI†), which may arise from their plasmonic coupling due to their approaching inside its constituent nanofibers. Secondly, as the temperature rises from 39 °C to 47 °C, close to the temperature range of the area change of the membrane, both their transverse and longitudinal plasmon bands are abruptly enhanced, thanks to the refractive index increase of the dispersed nanofibers after temperature induced phase transition. Thirdly, their maximum wavelengths are both red-shifted within the same temperature range, which could be due to two reasons. One is that the collapsed polymer network around the Au@AgNRs could increase their surrounding refractive index.³⁹ However, as investigated by Schmidt et al.,⁴⁰ this contribution to the wavelengths red-shift should be limited owing to slight variation of the refractive index before and after phase transition. Another is that temperature triggering phase transition of the composite nanofibers could reduce the distances between the loaded Au@AgNRs. As reported by Sánchez-Iglesias, in the gold-nanorod-pair system, side-to-side interactions lead to a red-shift of the transverse plasmon band and a blue-shift of the longitudinal plasmon band, while tip-to-tip ones would red-shift both bands.⁴¹ In our system, both the tip-to-tip and side-to-side distances between the Au@AgNRs should be shortened after temperature driven phase transition of their lodged nanofibers because of their directional alignment along the fibers axes, as above evidenced. However, it can be deduced from the red-shift of their longitudinal plasmon band that their tip-to-tip interactions is dominant over their side-to-side ones, due to the possibility that the longitudinal shrinkage percentage of the nanofibers is larger than the transverse one.

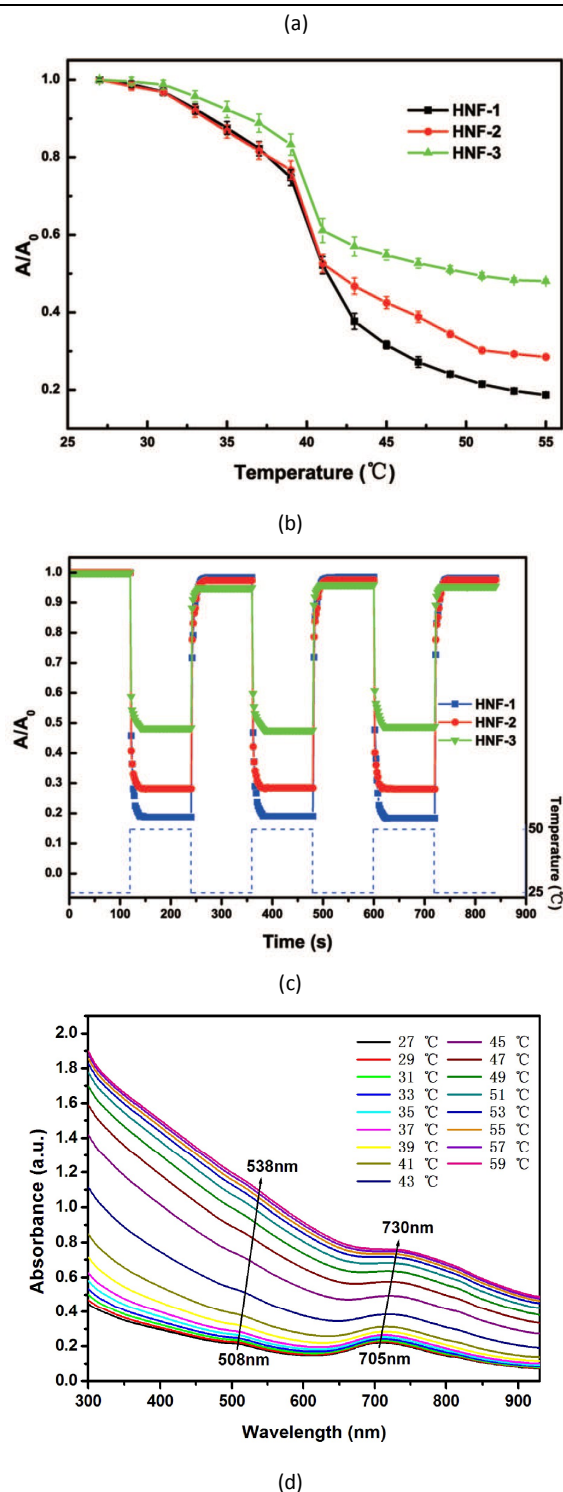
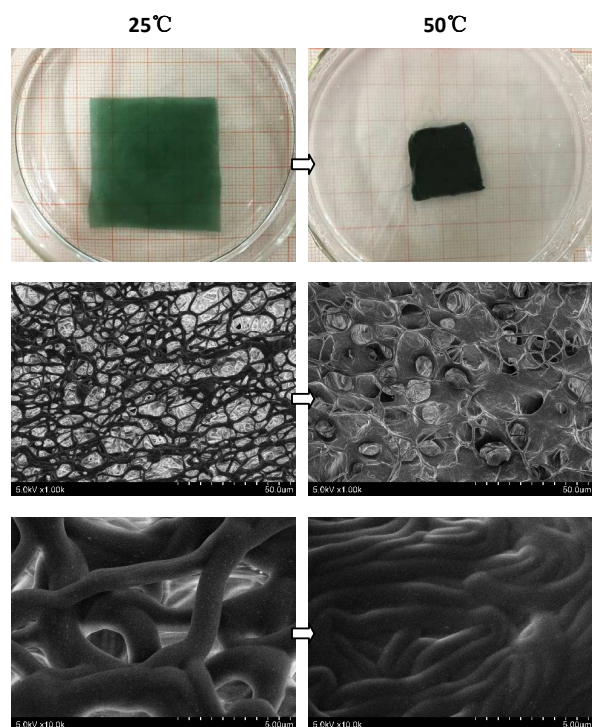


Fig. 3 (a) Optical images of HNF-2 immersed in 25 and 50 °C water and SEM images of the membranes prepared by liquid nitrogen freezing and then freeze drying. (b) Temperature-dependent area change of Au@AgNRs/PNN composite nanofibrous membranes (3.6 cm×3.6 cm) in pure water measured at a heating rate of 0.1 °C·min⁻¹. (c) Reversibility of time-dependent deswelling and swelling of Au@AgNRs/PNN composite nanofibrous membranes (3.6 cm×3.6 cm) immersed alternately in 25 °C or 50 °C water after 2 min. (d) UV-visible spectra of the nanofibers aqueous dispersion at

different temperatur

Use of Au@AgNRs/PNN composite nanofibrous membrane as SERS substrate and its temperature-tunable SERS efficiency

Compared to previously reported smart composite microgels,^{13,14} Au@AgNRs/PNN composite nanofibrous membrane should be more suitable for the use as SERS substrate because of its free-standing and flexible features.³⁶ Here, its SERS efficiency was evaluated using 4-NTP as a standard Raman active probe molecule. Fig. S6 (a) in the ESI† shows the SERS spectra of 4-NTP aqueous solution with the same concentration, obtained with three excitation wavelengths, i.e. 532 nm, 633 nm and 785 nm. The typical Raman peaks of 4-NTP are reflected in the spectra, including peaks at 1080 cm^{-1} , 1334 cm^{-1} and 1571 cm^{-1} , attributed to C–S stretching, O–N=O symmetric stretching and the phenyl ring stretching modes, respectively.⁴² From Fig. S6 (a) in the ESI†, we can see that the membrane as substrate exhibits the strongest SERS efficiency with the excitation wavelength of 785 nm, since it is the closest to the longitudinal plasmon resonance wavelength of its entrapped Au@AgNRs, resulting in the strongest surface electric field enhancement effect. Au@AgNRs/PNN composite nanofibrous membranes with three different Au@AgNRs contents were used as the substrates to measure the SERS spectra of 10^{-7} M 4-NTP aqueous solution at 25 °C, respectively, and the results are given in Fig. S6 (b) in the ESI†. The plot of their 1334 cm^{-1} peak intensities against the Au@AgNRs concentrations in their spinning solutions is depicted in Fig. S6 (c) in the ESI†. It can be viewed that their SERS efficiency is nearly proportionally increased with the Au@AgNRs concentration, revealing that their SERS efficiency comes from the bimetallic nanorods. Then, the composite nanofibrous membranes were used as the substrates to measure the SERS spectra of different concentrations of 4-NTP solution from 10^{-13} M to 10^{-7} M at 25 °C, respectively, and the result for HNF-2 is given in Fig. 4(a) and the others in Fig. S7 in the ESI†. With the increase of 4-NTP concentration, its SERS intensity is progressively raised. Even on HNF-1 substrate, the SERS signal of 10^{-12} M 4-NTP can be obviously observed (see Fig. S7(b) in the ESI†). If the membrane HNF-3 was used as a SERS substrate, 10^{-13} M 4-NTP in aqueous solution was able to be detected (Fig. S7 (e) in the ESI†). The plot of 1334 cm^{-1} peak intensities in Fig. 4(a) versus the logarithmic concentrations (log (c)) of 4-NTP is illustrated in Fig. 4(b), which can be fitted into a line with the correlation coefficient of 0.993 (n=9). This result shows that there is a good linear relationship between the SERS intensity and the logarithmic concentration of the analyte, indicating that the SERS signal based on Au@AgNRs/PNN composite nanofibrous membrane as substrate is highly reproducible. The high SERS signal reproducibility should arise from monodispersity and homogeneous distribution of the Au@AgNRs within its constituent nanofibers. In addition, fifteen times of measurements of 10^{-6} M 4-NTP aqueous solution were carried out on the same membrane (HNF-2), and the obtained SERS spectra are exhibited in Fig. 4(c). The estimated relative standard deviation (RSD) of the intensities of their 1334 cm^{-1} peaks is 3.87%, further confirming high reproducibility of the SERS signals from the membrane. These results mean that Au@AgNRs/PNN composite nanofibrous membrane could be

used as the SERS substrate for quantitative analysis.

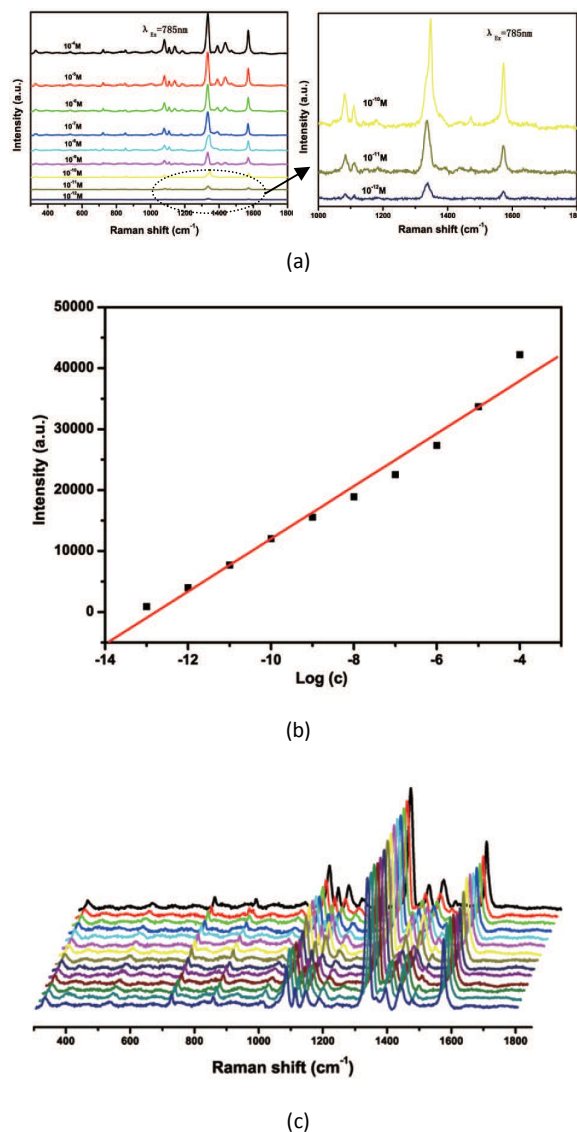
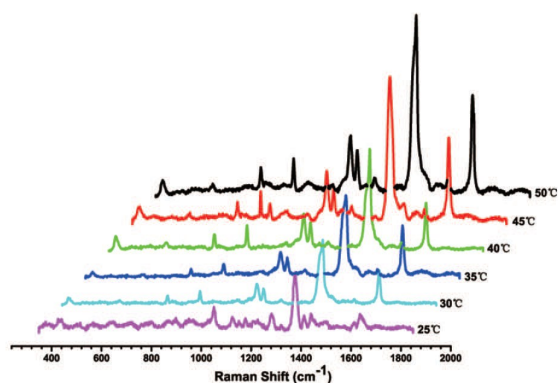


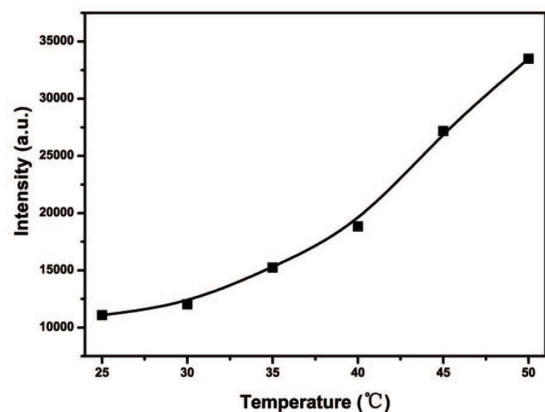
Fig. 4 (a) SERS spectra of different concentrations of 4-NTP in 25 °C aqueous solution based on HNF-2 as substrate with 785 nm laser excitation; (b) Plot of the SERS intensity of the 1334 cm^{-1} peak in (a) vs. log (c) of 4-NTP; (c) SERS spectra of 10^{-6} M 4-NTP acquired from 15 different spots on the membrane HNF-2.

The effect of temperature on the SERS efficiency of Au@AgNRs/PNN composite nanofibrous membrane was investigated using 10^{-9} M 4-NTP aqueous solution as the analyte, as illustrated in Fig. 5(a). One can observe that all peaks in its SERS spectrum are remarkably enhanced as the temperature is increased from 20 °C to 50 °C. The plot of the 1334 cm^{-1} peak intensity as a function of temperature is exhibited in Fig. 5(b). Its marked change occurs within the temperature range from 35 °C to 45 °C, in agreement with the one for the area change of the composite nanofibrous membrane with temperature. It can be inferred from the agreement that the temperature driven SERS signal enhancement possibly results from the plasmonic coupling

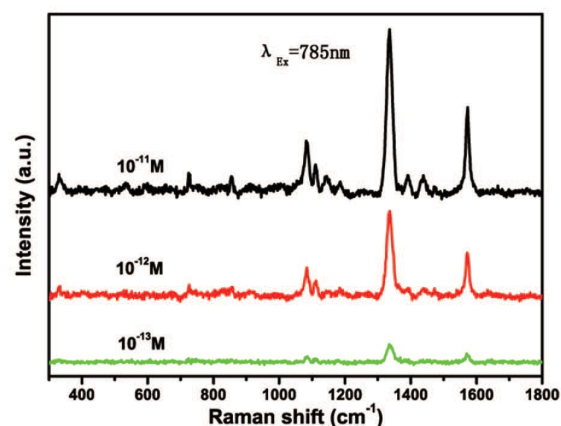
between the approached Au@AgNRs after temperature triggered adhesion between its constituent nanofibers, as previously discussed.¹³ This result implies that the detection sensitivity based on Au@AgNRs/PNN composite nanofibrous membrane as SERS substrate can be improved by elevating detection temperature. The estimation has been confirmed through SERS detecting 10^{-13} M 4-NTP in 50 μ aqueous solution using HNF-2 as substrate, as shown in Fig. 5(c) and (d). By comparing the results obtained at 25 $^{\circ}$ C and 50 $^{\circ}$ C, the low detection limit of 4-NTP at the high detection temperature is lowered one order of magnitude. Because of its fast thermo-response rate, swelling or deswelling equilibrium of the membrane as SERS substrate at each detection temperature can be shortly reached, which is helpful to shortening measurement time.



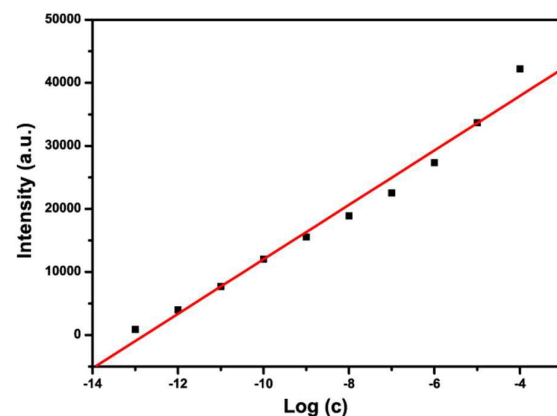
(a)



(b)



(c)



(d)

Fig. 5 (a) SERS spectra of 10^{-9} M 4-NTP aqueous solution using the membrane HNF-3 as substrate at different temperatures; (b) The 1334 cm^{-1} peak intensity in (a) as a function of temperature; (c) SERS spectra of different concentrations of 4-NTP in $50\text{ }^{\circ}\text{C}$ aqueous solution based on the membrane HNF-2 as substrate; (d) Plot of the intensity of the 1334 cm^{-1} peak in (c) vs. $\log(c)$ of 4-NTP

Application of Au@AgNRs/PNN composite nanofibrous membrane for in-situ SERS monitoring its catalyzed reaction

As reported recently,³¹ Au@AgNRs possess high catalytic activity and selectivity for some reactions, so it is expected that flexible free-standing Au@AgNRs/PNN composite nanofibrous membrane with macroscopic strength can be used for label-free in-situ SERS monitoring its catalyzed reaction. To validate the expectation, the reduction of 4-NTP into 4-aminothiophenol (4-ATP) by NaBH_4 in the presence of the membrane was selected as a model reaction, as schematically illustrated in Fig. 1 (b). The reaction can be considered as a two-step consecutive one (see Scheme S2 in the Supporting Information), either by a direct route via a hydroxylamine intermediate (4-thiolphenylhydroxylamine) or a condensation route through the formation of azobenzene intermediate (4,4'-dimercaptoazobenzene (4,4'-DMAB)).^{43,44} In the direct route, the nitro group of 4-NTP is reduced into nitroso, hydroxylamine, and amino groups successively. In the

condensation route, an azobenzene compound is generated as an intermediate from the condensation of a nitroso compound and a hydroxylamine compound, and it is finally reduced into two amino compounds. Therefore, detection of the intermediate is crucial to making clear the reaction mechanism. Fig. 6 displays the time dependent SERS spectra, which were recorded every 5 min interval after adding the NaBH_4 solution to 10^{-4} M 4-NTP solution containing the membrane (HNF-2) at 25°C (from top to bottom). In the SERS spectrum at its top, only the Raman peaks of 4-NTP are present. After addition of NaBH_4 , its peaks are gradually weakened and three new peaks at 1140, 1385 and 1427 cm^{-1} appear accordingly, which can be assigned to the C–N symmetric stretching, N=N stretching, and C–H in-plane bending modes of 4,4'-DMAB, respectively.⁴² Their intensities initially increase with reaction time (from black to green spectra) and then gradually decrease up to near-zero (from green to yellow ones), corroborating its character as an intermediate. In addition to the peaks of 4,4'-DMAB, a new peak at 1590 cm^{-1} shows up nearly simultaneously and gradually dominates the spectrum, which is attributed to the amino vibrational mode of the product 4-ATP. The results indicate that the reduction of 4-NTP into 4-ATP by NaBH_4 , catalyzed by Au@AgNRs/PNN composite nanofibrous membrane, proceeds via a condensation route. The mechanism can be explained by the speculation that the transformation of 4-NTP to 4,4'-DMAB may be caused by plasmon-induced charge transfer under the laser irradiation.⁴⁵ Concretely, the reaction could be catalyzed via electron transfer between laser irradiation induced plasmon resonance surface of Au@AgNR and the nitro group of 4-NTP through the molecule, because of its chemisorption on the Ag surface by its thiol group.

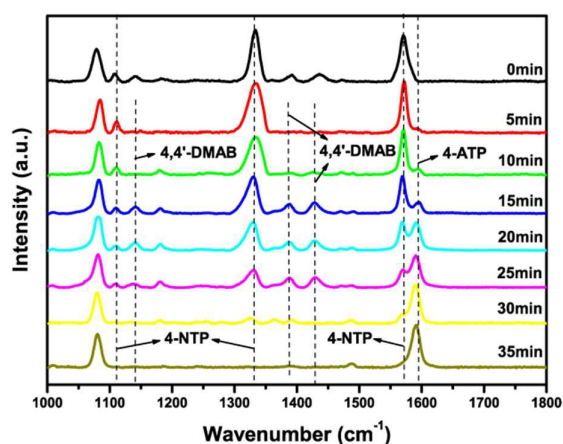


Fig. 6 SERS spectra for in-situ monitoring the reduction of 4-NTP catalyzed by the membrane HNF-2

Conclusion

In summary, monodisperse Au@AgNRs were successfully loaded into thermo-responsive nanofibrous membrane via electrospinning process, followed by heat treatment. The prominent structural feature of the produced composite nanofibrous membrane is oriented alignment of the nanorods

along the axes of its constituent fibers, so their tip-to-tip and side-to-side interactions can be tuned by temperature, resulting in their temperature-tunable plasmonic property. Compared to the previously reported thermo-responsive composite materials based on thermo-responsive bulky hydrogels or microgels, the composite nanofibrous membrane has both fast thermo-response and macroscopic mechanical strength. It can be used as a smart free-standing SERS substrate with high signal reproducibility for quantitative analysis, and its SERS efficiency can be increased by elevating temperature. Moreover, the composite nanofibrous membrane has the ability to in-situ SERS monitor its catalyzed reaction, which is beneficial to understanding the reaction mechanism.

Acknowledgements

The authors are grateful to the National Natural Science Foundation of China (51373030, 51503033) and the Fundamental Research Funds for the Central Universities (2232014D3-43). They gratefully acknowledge Prof. S. Agarwal of Universität Bayreuth for her valuable suggestions.

Notes and references

- 1 M. A. C. Stuart, W. T. S. Huck, J. Genzer, M. Mueller, C. Ober, M. Stamm, G. B. Sukhorukov, I. Szleifer, V. V. Tsukruk, M. Urban, F. Winnik, S. Zauscher, I. Luzinov and S. Minko, *Nat. Mater.*, 2010, **9**, 101-113.
- 2 H. Zhang, J. S. Han and B. Yang, *Adv. Funct. Mater.*, 2010, **20**, 1533-1550.
- 3 X. H. Li, G. Y. Chen, L. B. Yang, Z. Jin and J. H. Liu, *Adv. Funct. Mater.*, 2010, **20**, 2815-2824.
- 4 M. Molina, M. Asadian-Birjand, J. Balach, J. Bergueiro, E. Miceli and M. Calderon, *Chem. Soc. Rev.*, 2015, **44**, 6161-6186.
- 5 M. Karg, *Colloid. Polym. Sci.*, 2012, **290**, 673-688.
- 6 I. Tokarev and S. Minko, *Soft Matter*, 2012, **8**, 5980-5987.
- 7 R. Messing and A. M. Schmidt, *Polym. Chem.*, 2011, **2**, 18-32.
- 8 S. G. Cao, B. H. Hu and H. Q. Liu, *Polym. Int.*, 2009, **58**, 545-551.
- 9 S. H. Jiang, F. Y. Liu, A. Lerch, L. Ionov and S. Agarwal, *Adv. Mater.*, 2015, **27**, 4865-4870.
- 10 J. Perez-Juste, I. Pastoriza-Santos and L. M. Liz-Marzan, *J. Mater. Chem. A*, 2013, **1**, 20-26.
- 11 M. Karg and T. Hellweg, *J. Mater. Chem.*, 2009, **19**, 8714-8727.
- 12 Y. Y. Liu, X. Y. Liu, J. M. Yang, D. L. Lin, X. Chen and L. S. Zha, *Colloid Surf. A: Physicochem. Eng. Asp.*, 2012, **393**, 105-110.
- 13 X. Y. Liu, X. Q. Wang, L. S. Zha, D. L. Lin, J. M. Yang, J. F. Zhou and L. Zhang, *J. Mater. Chem. C*, 2014, **2**, 7326-7335.
- 14 X. Y. Liu, C. Zhang, J. M. Yang, D. L. Lin, L. Zhang, X. Chen and L. S. Zha, *RSC Adv.*, 2013, **3**, 3384-3390.
- 15 X. Dong, X. B. Zou, X. Y. Liu, P. Lu, J. M. Yang, D. L. Lin, L. Zhang and L. S. Zha, *Colloid Surf. A: Physicochem. Eng. Asp.*, 2014, **452**, 46-50.
- 16 C. B. Huang, S. J. Soenen, J. Rejman, B. Lucas, K. Braeckmans, J. Demeester and S. C. De Smedt, *Chem. Soc. Rev.*, 2011, **40**, 2417-2434.
- 17 S. Ramakrishna, K. Fujihara, W. E. Teo, T. Yong, Z. W. Ma and R. Ramaseshan, *Mater. Today*, 2006, **9**, 40-50.
- 18 I. D. Kim, A. Rothschild, B. H. Lee, D. Y. Kim, S. M. Jo and H. L. Tuller, *Nano Lett.*, 2006, **6**, 2009-2013.

- 19 C. L. Zhang and S. H. Yu, *Chem. Soc. Rev.*, 2014, **43**, 4423-4448.
- 20 F. Mitschang, H. Schmalz, S. Agarwal and A. Greiner, *Angew. Chem. Int. Edit.*, 2014, **53**, 4972-4975.
- 21 W. E. Teo and S. Ramakrishna, *Nanotechnology*, 2006, **17**, R89-R106.
- 22 C. Huang, S. J. Soenen, J. Rejman, B. Lucas, K. Braeckmans, J. Demeester and S. C. De Smedt, *Chem. Soc. Rev.*, 2011, **40**, 2417-2434.
- 23 R. B. Jiang, H. J. Chen, L. Shao, Q. Li and J. F. Wang, *Adv. Mater.*, 2012, **24**, OP200-OP207.
- 24 Z. Y. Bao, D. Y. Lei, R. B. Jiang, X. Liu, J. Y. Dai, J. F. Wang, H. L. W. Chan and Y. H. Tsang, *Nanoscale*, 2014, **6**, 9063-9070.
- 25 E. C. Cho, P. H. C. Camargo and Y. N. Xia, *Adv. Mater.*, 2010, **22**, 744-748.
- 26 X. Dong, J. F. Zhou, X. Y. Liu, D. L. Lin and L. S. Zha, *J. Raman Spectrosc.*, 2014, **45**, 431-437.
- 27 T. N. A. Dao, P. Singh, C. Shankar, D. Mott and S. Maenosono, *Appl. Phys. Lett.*, 2011, **99**, 073107.
- 28 M. Erol, Y. Han, S. K. Stanley, C. M. Stafford, H. Du and S. Sukhishvili, *J. Am. Chem. Soc.*, 2009, **131**, 7480-7481.
- 29 X. Guo, Q. Zhang, Y. H. Sun, Q. Zhao and J. Yang, *ACS Nano*, 2012, **6**, 1165-1175.
- 30 S. Jayabal and R. Ramaraj, *Appl. Catal. A-Gen.*, 2014, **470**, 369-375.
- 31 A. Monga and B. Pal, *Colloid Surf. A: Physicochem. Eng. Asp.*, 2015, **481**, 158-166.
- 32 X. Ye, C. Zheng, J. Chen, Y. Gao, C. B. Murray, *Nano Lett.* 2013, **13**, 765-771.
- 33 L. N. Chen, Y. C. Chiu, J. J. Hung, C. C. Kuo and W. C. Chen, *Macromol. Chem. Phys.*, 2014, **215**, 286-294.
- 34 W. D. Zhang, W. Zhang, N. C. Zhou, Z. P. Cheng, J. Zhu and X. L. Zhu, *Polymer*, 2008, **49**, 4569-4575.
- 35 C. D. Saquing, J. L. Manasco and S. A. Khan, *Small*, 2009, **5**, 944-951.
- 36 C. L. Zhang, K. P. Lv, H. P. Cong and S. H. Yu, *Small*, 2012, **8**, 648-653.
- 37 C. Wu, S. Q. Zhou, S. C. F. Auyeung and S. H. Jiang, *Angew. Makromol. Chem.*, 1996, **240**, 123-136.
- 38 R. Yoshida, K. Uchida, Y. Kaneko, K. Sakai, A. Kikuchi, Y. Sakurai and T. Okano, *Nature*, 1995, **374**, 240-242.
- 39 H. X. Xu, J. Xu, Z. Y. Zhu, H. W. Liu and S. Y. Liu, *Macromolecules*, 2006, **39**, 8451-8455.
- 40 S. Schmidt, H. Motschmann, T. Hellweg and R. von Klitzing, *Polymer*, 2008, **49**, 749-756.
- 41 A. Sanchez-Iglesias, M. Grzelczak, J. Perez-Juste and L. M. Liz-Marzan, *Angew. Chem. Int. Edit.*, 2010, **49**, 9985-9989.
- 42 G. C. Zheng, L. Polavarapu, L. M. Liz-Marzan, I. Pastoriza-Santos and J. Perez-Juste, *Chem. Commun.*, 2015, **51**, 4572-4575.
- 43 A. Grirrane, A. Corma and H. Garcia, *Science*, 2008, **322**, 1661-1664.
- 44 A. Corma, P. Concepcion and P. Serna, *Angew. Chem. Int. Edit.*, 2007, **46**, 7266-7269.
- 45 W. Xie, B. Walkenfort and S. Schluecker, *J. Am. Chem. Soc.*, 2013, **135**, 1657-1660.